A EUROPEAN JOURNAL

CHEMPHYSCHEM

OF CHEMICAL PHYSICS AND PHYSICAL CHEMISTRY

Accepted Article

Title: Odd–Even Effect on Luminescence Properties of Europium Aliphatic Dicarboxylate Complexes

Authors: Israel Assunção, Albano Carneiro, Renaldo Moura Jr., Cássio Pedroso, Ivan Guide Nunes Silva, Maria Felinto, Ercules Teotonio, Oscar Malta, and Hermi Brito

To be cited as: *ChemPhysChem* 10.1002/cphc.201900603

Link to VoR: http://dx.doi.org/10.1002/cphc.201900603

A Journal of

ChemPubSoc Europe

WILEY-VCH

www.chemphyschem.org

WILEY-VCH

FULL PAPER

Odd–Even Effect on Luminescence Properties of Europium Aliphatic Dicarboxylate Complexes

Israel P. Assunção,[a] Albano N. Carneiro Neto,[b][c] Renaldo T. Moura Jr.,[d] Cássio C. S. Pedroso,[a] Ivan G. N. Silva,[a] Maria C.F.C. Felinto,[e] Ercules E.S. Teotonio,[f] Oscar L. Malta,*[b] Hermi F. Brito *[a]

Abstract: The odd–even effect in luminescent $[Eu_2(L)_3(H_2O)_x]\cdot y(H_2O)$ complexes with aliphatic dicarboxylate ligands (L: OXA, MAL, SUC, GLU, ADP, PIM, SUB, AZL, SEB, UND, and DOD, where x = 2–6 and y = 0–4), prepared by the precipitation method, was observed for the first time in lanthanide compounds. The final dehydration temperatures of the Eu^{3+} complexes show a *zigzag* pattern as a function of the carbon chain size of the dicarboxylate ligands, leading to the so-called odd–even effect. The FTIR data confirmed the ligand-metal coordination *via* the mixed mode of bridge-chelate coordination, except for the Eu^{3+}–oxalate complex. XRD results point out to highly crystalline materials belonging to the monoclinic system. The odd–even effect on the 4f-4f luminescence intensity parameters (Ω_2 and Ω_4) was explained by using an extension of the Dynamic Coupling mechanism, herein named the Ghost-Atom model. In this method, the long-range polarizabilities (α^*) were simulated by a Ghost-Atom located at the middle of each ligand chain. The values of α^* were estimated using the localized molecular orbital approach. The emission intrinsic quantum yield (Q_{Ln}^{Ln}) of the Eu^{3+} complexes also presented an the odd–even effect, successfully explained in terms of the *zigzag* behavior showed by the Ω_2 and Ω_4 intensity parameters. Luminescence quenching due to water molecules in the first coordination sphere was discussed and rationalized.

[a] Dr. Israel P. Assunção, Dr. Cássio C. S. Pedroso, Dr. Ivan G. N. Silva, Prof. Hermi F. Brito
Department of Fundamental Chemistry
Institute of Chemistry, University of São Paulo
Av. Prof. Lineu Prestes, São Paulo - SP, 05508-000, Brazil.

[b] Dr. Albano N. Carneiro Neto, Prof. Oscar L. Malta
Department of Fundamental Chemistry.
Federal University of Pernambuco
Av. Prof. Moraes Rego, Recife - PE, 50670-901, Brazil.
E-mail: oscar.malta@ufpe.br

[c] Dr. Albano N. Carneiro Neto
Physics Department and CICECO – Aveiro Institute of Materials
University of Aveiro
Campus Universitário de Santiago, Aveiro, 3810-193, Portugal.

[d] Prof. Renaldo T. Moura Jr.
Department of Chemistry and Physics
Federal University of Paraíba, Campus II
Cidade Universitária, Areia - PB, 58397-000 Brazil.

[e] Prof. Maria C.F.C. Felinto
Nuclear and Energy Research Institute - IPEN/CNEN
Av. Prof. Lineu Prestes, São Paulo - SP, 05508-000, Brazil.

[f] Prof. Ercules E.S. Teotonio
Department of Chemistry
Federal University of Paraíba
Jardim Universitário, - João Pessoa - PB, 58051-970, Brazil.

Supporting information for this article is given via a link at the end of the document.

Introduction

The aliphatic α,ω,-alkanedicarboxylate anions ($^-OOC–(CH_2)_{n-2}–COO^-$, 2 ≤ n ≤ 12) (Figure 1) have very interesting features such as their versatile coordination modes, for example monodentate, chelated bidentate, bridging or mixed modes.[1] The coordination modes can lead to different multidimensional structures depending mostly on the length and flexibility of the chain.[1,2] In addition, there are other intrinsic physico-chemical properties of the α,ω,-alkanedicarboxylic acids due to the odd–even effect, which is quite well established in the literature.[3–5] This effect plays an important role in the regular variations of different properties of compounds: melting points,[3,5,6] solubility,[3] nanocalorimetry,[7] electrochemical,[8,9] the emulsifying ability of some surfactants[9] or structural self-assembling.[8,10–12] It is noteworthy that the odd–even effect arises from a difference in the packing mode between odd–odd or even–even carbon members of a given homologous series.[4–6,13]

According to the "parallelogram-trapezoid model" proposed by Thalladi *et al.*,[3] the even carbon members are arranged in such a way that the repulsive interactions between chains are decreased, leading to a more stable packing pattern. On the other hand, the odd carbon members possess some intrinsic higher energy that may be released in a process, for exemple dissolution or melting. This can explain why the odd carbon chains have higher solubilities and lower melting points than their even carbon members. Besides, a nanoindentation study on α,ω-alkanedicarboxylic acids has demonstrated that the elastic modulus presents an odd–even conformation similar to the melting temperature.[5]

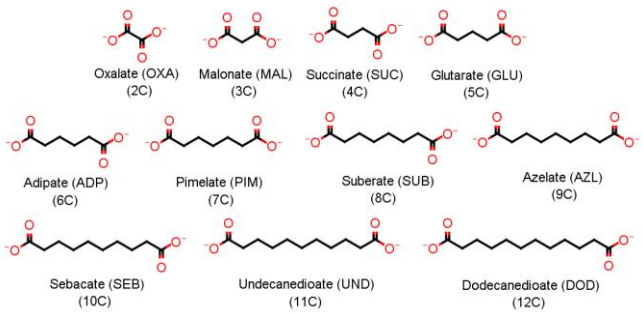

Figure 1. Structural formulas of eleven different aliphatic α,ω,-alkanedicarboxylate anions –OOC–(CH2)n-2–COO–, in which 2 ≤ n ≤ 12.

The odd–even effect has been used in studies of self-assembled monolayers (SAMs) and fully controls the ability of molecules to form highly ordered structures such as the effect in molecular self-assembled packing.[8,11,12,14] This *zigzag*

conformation[2] plays a key role in the structural organization of SAMs based on carboxylic acid structures,[4,15] which present a potential for molecular electronic applications.

The last decades have seen, a significant increase in interest in trivalent lanthanides (Ln^{3+}) coordination compounds with organic ligands[16–18] due to the great potential for a variety of applications such as gas storage,[19] catalyses,[20] medical uses,[21] and optical markers.[22] The luminescence properties of the Ln^{3+} ions are mostly dependent on their unique energy level structures. The 4f orbitals are effectively shielded from the chemical environment by the filled 5s and 5p sub-shells,[23] leading to narrow absorption and emission lines, maintaining more or less their atomic character. The 4f–4f transitions are parity forbidden by Laporte's rule, yielding very low absorptivity coefficients. This spectroscopic disadvantage is overcome by using organic ligand as an efficient luminescence sensitizer to absorb and efficiently energy transfer to the Ln^{3+} ions.[24]

The great advantage of using the Eu^{3+} ion as a luminescent probe is mainly due to its spectroscopic features: *i*) the principal emitting $^5D_0$ level is non-degenerate and presents a long luminescence decay time (milliseconds) and *ii*) the radiative rate of the $^5D_0 \rightarrow {}^7F_1$ transition, allowed by the magnetic dipole mechanism, is essentially insensitive to the ligand field environment and can be used as a reference transition to calculate spectroscopic parameters from the $^5D_0 \rightarrow {}^7F_{2,4,6}$ transitions.[24,25] From the emission and excitation spectra of Eu^{3+} complexes, unique information on the ligand field splitting, intramolecular energy transfer processes, intrinsic emission quantum yields, and overall luminescence quantum yields can be obtained.

Among the Ln^{3+} carboxylate compounds, the so-called Metal-Organic Frameworks (MOFs) have been receiving special attention in the fields of crystal engineering and molecular topology owing to the facility of synthesis and the possibility of modeling materials with desired properties. Most studies reported in the literature have focused on the synthesis and luminescent or magnetic properties of the Ln^{3+} coordination compounds.[26–28] Systematic studies on the correlation between the structural characteristics of the aliphatic dicarboxylate ligands and the luminescent properties of these complexes are still scarce.

In this work, we described the elucidation of the odd–even effect on the photoluminescence features of Eu^{3+} dicarboxylate complexes. Accordingly, we present the synthesis, characterization as well as the experimental and theoretical photoluminescence studies of a class of compounds with the general formula $[Eu_2(L)_3(H_2O)_x]\cdot y(H_2O)$, where L refers to dicarboxylate ligands $^-OOC–(CH_2)_{n-2}–COO^-$, in which $2 \le n \le 12$, with $x = 2–6$ and $y = 0–4$, depending on ligand. As far as we know, this is the first time that the odd–even effect is observed and rationalized in the luminescence features of lanthanide compounds. The theoretical treatment is based on previous approaches on 4f-4f intensities.[29–31] The *zigzag* patterns were successfully explained by the proposal of an extension of the Dynamic Coupling mechanism to describe the intensities of 4f-4f transitions. A model, herein called the "Ghost-Atom" model, was used to simulate the long-range dispersion effects of the ligand chain on the first coordination sphere of the trivalent europium complexes.

The coordination compounds were characterized by elemental analysis, X-ray powder diffraction, thermogravimetric analysis, and UV−visible luminescence. It is noteworthy that the analogs La^{3+} and Gd^{3+} complexes were prepared with the objective of obtaining information on $O^{2-}(2p) \rightarrow Eu^{3+}(4f)$ Ligand-to-Metal Charge Transfer (LMCT) states and triplet states (T_1) of the dicarboxylate ligands, respectively.

Experimental Section

Synthesis of the $[Ln_2(L)_3(H_2O)_x]\cdot y(H_2O)$ Complexes

The dicarboxylic acids (H_2OXA, H_2MAL, H_2SUC, H_2GLU, H_2ADP, H_2PIM, H_2SUB, H_2AZL, H_2SEB, H_2UND, and H_2DOD) were purchased from Sigma-Aldrich and used without previous treatment. The lanthanides chlorides ($LnCl_3\cdot 6H_2O$) were prepared by a reaction between their corresponding lanthanides oxides, Ln_2O_3 (99.999%) (Ln: La^{3+}, Eu^{3+}, and Gd^{3+}) from CSTARM and concentrated hydrochloric acid (37%, Merck).

The synthetic procedure of the Ln^{3+} aliphatic α,ω,-alkanedicarboxylate complexes reported in the literature have been obtained predominantly by the hydrothermal method,[1,32,33] while there are a few works reporting on the precipitation method.[34] In the present work, some modifications in the precipitation method were performed, such as the Ln^{3+} solutions addition to a heated solution at ~80 ºC of the previously deprotonated ligand (pH ~ 7) in order to increase the solubility of the ligands in water (yields 90%). The general reaction can be represented by Eq. (1).

$$2[LnCl_3(H_2O)_6](aq) + 3Na_2L(aq) \rightarrow [Ln_2(L)_3(H_2O)_x]\cdot y(H_2O)(s) + 6Na^+(aq) + 6Cl^-(aq) \quad (1)$$

Characterization Techniques

The elemental analyses were performed in a Perkin-Elmer CHN 2400 instruments. The infrared absorption spectra of the compounds were measured using KBr pellets on a Bomem MB100 FTIR spectrometer from 400 to 4000 cm^{-1} with a spectral resolution of 4.0 cm^{-1}. Thermogravimetric curves from 25 to 800 ºC were performed on a 2950 TGA HR V5.4A under dynamic synthetic air atmosphere of 50 $cm^3\cdot min^{-1}$ with a constant heating rate of 3 ºC·min^{-1}. The X-ray diffraction patterns were obtained with a Miniflex Rigaku diffractometer using $CuK_{\alpha 1}$ radiation (30 kV and 15 mA) in the (2θ) 3 to 60º range and of 0.05 s of pass time.

The diffuse reflectance data were collected with a Shimadzu UV-2600 equipment spectrophotometer containing an integrating sphere. $BaSO_4$ was used as the diffuse reflectance standard. Steady-state excitation and emission spectra of the Eu^{3+} complexes and the time-resolved phosphorescence spectra of the Gd^{3+} complexes in solid state at room (~300 K) and liquid nitrogen (77 K) temperatures were recorded at an angle of 22.5º (front face) with a spectrofluorimeter (SPEX-Fluorolog 2) with double grating between 0.5 and 2.0 mm monochromator (SPEX1680), and a 450 W Xenon lamp as excitation source. All spectra were recorded using a detector mode correction. The luminescence decay curves of the emitting levels of the $[Eu_2(L)_3(H_2O)_x]\cdot y(H_2O)$ were measured at room temperature, while the analogous Gd^{3+} complexes were measured at low temperature (77 K), using a phosphorimeter SPEX 1934D accessory coupled to the spectrofluorometer.

Experimental Intensity Parameters

The experimental intensity parameters (Ω_2 and Ω_4) can be calculated according to Eq (2),[35,36]

$$\Omega_\lambda = \frac{3\hbar c^3 A_{0\to\lambda}}{4e^2\omega^3\chi\left\langle {}^7F_\lambda \| U^{(\lambda)} \| {}^5D_0 \right\rangle^2} \quad (2)$$

where $\chi = n_{ref}\left(n_{ref}^2+2\right)^2/9$ is the Lorentz local field correction and n_{ref} is the linear refractive index of the medium (assumed 1.5 for these complexes). ω is the angular frequency of the transition. The $\left\langle {}^7F_\lambda \| U^{(\lambda)} \| {}^5D_0 \right\rangle^2$ are the square reduced matrix elements and the values for these quantities are equal to 0.0032 and 0.0023 for $\lambda = 2$ and 4, respectively.[37] The $A_{0\to J}$ are spontaneous emission coefficients assigned to the $^5D_0 \to {}^7F_J$ transitions. The $^5D_0$ ($^7F_1$ transition is governed practically 100% by the Magnetic Dipole mechanism, thus its spontaneous emission coefficient is formally insensitive to the chemical environment (,-0→ 1.~ 50–80 s^{-1}). Therefore, it is taken as an internal standard to determine the $A_{0\to J}$ values for Eu^{3+} complexes using Eq. (3),[24,36]

$$A_{0\to J} = \left(\frac{S_{0\to J}}{S_{0\to 1}}\right) A_{0\to 1} \quad (3)$$

where $S_{0\to 1}$ and $S_{0\to J}$ correspond to the areas under of the emission curves (proportional to the number of the emitted photons) of the $^5D_0 \to {}^7F_1$ and $^5D_0 \to {}^7F_{2,4,6}$ transitions, respectively. The $^5D_0 \to {}^7F_6$ transition is frequently not observed experimentally.[36]

Theoretical Section

Theoretical Intensity Parameters

The theoretical intensity parameters Ω_λ (λ=2, 4, and 6) of 4f-4f transitions (from the Judd-Ofelt theory[38,39]) depend on the chemical environment and on the lanthanide ion. The two main contributions to the description of spontaneous emission coefficients are the Forced Electric Dipole (FED)[38,39] and the polarizability dependent Dynamic Coupling (DC)[40–42] mechanisms. The theoretical parameters Ω_λ's are given by Eqs. (4–7),

$$\Omega_\lambda = (2\lambda+1)\sum_{t,p}\frac{\left|B_{\lambda tp}\right|^2}{(2t+1)} \quad (4)$$

where

$$B_{\lambda tp} = B_{\lambda tp}^{\mathrm{FED}} + B_{\lambda tp}^{\mathrm{DC}} \quad (5)$$

$$B_{\lambda tp}^{\mathrm{FED}} = \frac{2}{\Delta E}\langle \mathrm{r}^{t+1}\rangle \Theta(\mathrm{t},\lambda)\gamma_p^t \quad (6)$$

$$B_{\lambda tp}^{DC} = -\left[\frac{(\lambda+1)(2\lambda+3)}{(2\lambda+1)}\right]^{\frac{1}{2}}\langle r^\lambda\rangle\langle f\|C^{(\lambda)}\|f\rangle\Gamma_p^t\delta_{t,\lambda+1} \quad (7)$$

with t (t = 1, 3, 5, and 7) and p being the ranks and components, respectively, that define the spherical harmonics Y_p^{t*} in Eqs. (8 and 9). The magnitudes of the γ_p^t and Γ_p^t terms are dependent on the chemical bond, structure, and nature of the chemical environment of the lanthanide ion:

$$\gamma_p^t = e^2\left(\frac{4\pi}{2t+1}\right)^{1/2}\sum_j \rho_j g_j \left(2\beta_j\right)^{t+1}\frac{Y_p^{t*}(\theta_j,\varphi_j)}{R_j^{t+1}} \quad (8)$$

$$\Gamma_p^t = \left(\frac{4\pi}{2t+1}\right)^{1/2}\sum_j \left[\left(2\beta_j\right)^{t+1}\alpha_{OP_j} + \alpha_j'\right]\frac{Y_p^{t*}(\theta_j,\varphi_j)}{R_j^{t+1}} \quad (9)$$

where ρ_j are the overlap integrals between valence orbitals of the Ln and ligating atoms (or ions), g_j are charge factors, R_j are the equilibrium distances between Ln^{3+} ion and the ligating atoms or ions, and $\beta_j = \left(1+\rho_j\right)^{-1}$. Eqs. (8 and 9) are derived from the Simple Overlap Model (SOM)[29,30] for the Ligand Field and Bond Overlap Model (BOM)[31,43] for the Dynamic Coupling mechanism, respectively. The polarizability is partitioned into two terms: the polarizability α_{OP_j} associated with the overlap in the chemical bond and α_j' associated to the moieties of the ligand polarizability locally influencing the Ln^{3+} ion.

The α_{OP_j} values can be calculated by Eq. (10) as a function of the R_j, the first excitation energy $\Delta\varepsilon_j$, and ρ_j.[44] Details on these quantities in Eqs. (4-10) are reported in the work of Moura Jr. *et al.*[31]

$$\alpha_{OP_j} = \frac{e^2\rho_j^2 R_j^2}{2\Delta\varepsilon_j} \quad (10)$$

It is conceived that the charge distribution localized in the chemical bond and on the organic ligands makes significant contributions to the ligand field in Eu^{3+} compounds.[45] The contributions to the molecular polarizability of Localized Molecular Orbitals (LMOs) can be used to estimate the isolated ligand effective polarizability α_j'. The localization of canonical molecular orbitals can be performed by different procedures, being the Pipek–Mezey approach[46] quite successful in providing LMOs for the ligands of interest.[31]

The Odd–Even Effect in the Intensity Parameters

The odd–even effect of the Eu^{3+}–dicarboxylate complexes can be explained in terms of an approach named the "Ghost–Atom" model, as mentioned above. This model presumes that a species located at the middle of the ligand chain has the purpose of simulating the effect of the whole ligand on the first coordination sphere of the Eu^{3+} complex. It is important to emphasize that this approach also takes into account the *zigzag* alternation in the aliphatic dicarboxylate chain, being an extension of the Bond Overlap Model.[31]

The Ghost–Atom Model

The way the effective polarizability α' has been calculated does not consider the presence of the effective charge of the Eu^{3+} ion. Clearly, the α' takes only into account the short-range coordination polyhedron polarization in the COO^- carboxylate

group. The long-range ligand contributions should be included in the DC mechanism by the aliphatic chain LMOs polarizabilities.

The long-range interactions of the aliphatic carbon chain LMOs polarizabilities α_v^*, given by Eq. (11), are accounted as a representation of an atom, labeled as the Ghost–Atom (GA), located at the middle of the dicarboxylate ligand chain. It is important to highlight that the GA makes long-range contributions to the first coordination sphere:

$$\alpha_v^* = \sum_h \alpha_h^{LMO} e^{-d_h} \tag{11}$$

d_h is the distance between the GA and the h-th LMO polarizability α_h^{LMO}. The GA polarizability (α^*) is calculated as the sum of polarizabilities multiplied by an exponential decay factor over the distance (d_h) of the GA to the center of each LMO (Figures S1a and S1b).

The inclusion of α_v^* in the DC mechanism can be done adding a term in Eq. (9) in the following form:

$$\Gamma_p^t = \left(\frac{4\pi}{2t+1}\right)^{1/2} \left[\sum_j \left[(2\beta_j)^{t+1} \alpha_{OP_j} + \alpha'_j \right] \frac{Y_p^{t*}(\theta_j, \varphi_j)}{R_j^{t+1}} + \sum_v \alpha_v^* \frac{Y_p^{t*}(\theta_v, \varphi_v)}{R_v^{t+1}} \right] \tag{12}$$

in which v represents the GA. It must be highlighted that the GA represents induced point dipole moments, consequently without direct covalency effects in the first coordination sphere.

An illustration of the aliphatic dicarboxylate ligands with an odd (a) and even (b) carbon members of the chain is depicted in Figure 2. The symmetry of the dicarboxylate ligands imposes the condition that the vectors illustrated by the same numerical labels (in the same ligand) have the same magnitudes and chemical environments. It can be perceived that the odd and even carbon members have permanent dipole moments $\vec{\mu}_P \neq 0$ and $\vec{\mu}_P \approx 0$, respectively (Figures 2a and 2b).

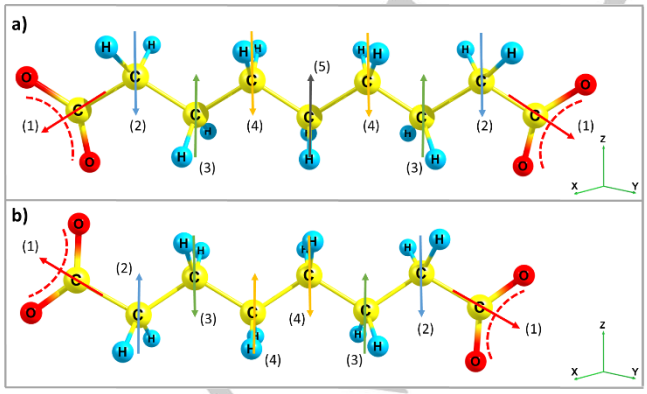

Figure 2. Vector contribution of partial dipole moments of the dicarboxylate ligands. (a) For odd members (n=9) the resultant permanent dipole moment is $\vec{\mu}_P \neq 0$ and (b) for even members (n=8) $\vec{\mu}_P \approx 0$. The dashed line (in the carboxylate groups) represents the delocalized charge.

The GA average distances (R_v) to the Eu^{3+} ion (Figure S1c) are proportional to the carbon chain length, making Eq. (12) less dependent on the α_v^* values for long chains.

Results and Discussion

Characterization

The elemental analysis data of the Ln^{3+} coordination compounds (Ln: Eu^{3+} and Gd^{3+}) are in agreement with the formula $[Ln_2(OXA)_3(H_2O)_6]\cdot 4(H_2O)$, $[Ln_2(L)_3(H_2O)_6]$ (L: MAL and GLU), $[Ln_2(SUC)_3(H_2O)_2]\cdot H_2O$, $[Ln_2(ADP)_3(H_2O)_4]\cdot H_2O$, $[Ln_2(L)_3(H_2O)_4]$ (L: PIM, SUB, AZL, SEB, UND, DOD) (Table S1).

The thermogravimetric (TG) curves (Figure S2a-S2k) of the Eu^{3+} and Gd^{3+} dicarboxylate complexes recorded at the temperature interval from 25 to 800 °C corroborate with the elemental analysis data. All complexes with the same ligands and different Ln^{3+} ion present similar thermal decomposition profiles, indicating the same stoichiometry. The Ln^{3+} complexes with OXA, SUC, and ADP ligands present both coordinated and hydration water molecules in their structures, while the other remaining complexes presented only coordinated water molecules. In general, the Eu^{3+} dicarboxylate complexes showed relative lower decomposition temperatures compared with those Gd^{3+} complexes, reflecting the weaker interaction between the europium ion and the ligands.

TG curves show that increasing the carbon chain of the dicarboxylate ligands, the dehydration temperature (Figure 3) decreases due to increasing hydrophobic character of the complex. Interestingly, Figure 3 shows the *zigzag* pattern from the final temperatures of released H_2O molecules as a function of the number of carbon atoms ($2 \leq n \leq 12$) in the dicarboxylate ligands.

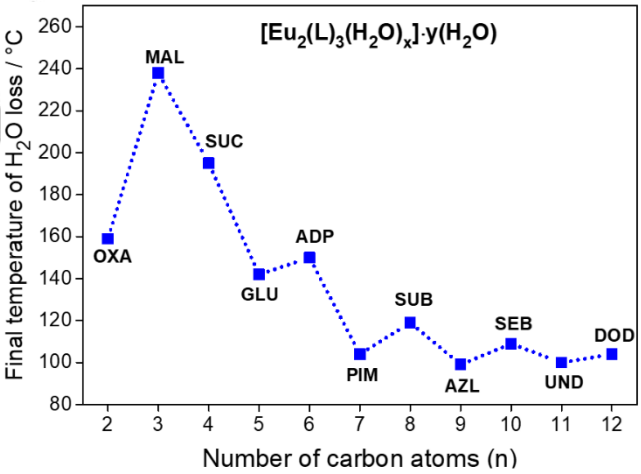

Figure 3. *Zigzag* pattern obtained from final temperature (°C) of released H_2O molecules as a function of the number of carbon atoms in the dicarboxylate ligands in $[Eu_2(L)_3(H_2O)_x]\cdot y(H_2O)$ complexes (L: $^-OOC(CH_2)_{n-2}COO^-$, $2 \leq n \leq 12$, x = 2–6, and y = 0–4).

FTIR spectra of the Eu^{3+}–dicarboxylate complexes (Figure S3) show a broad absorption band among 3000–3800 cm^{-1} centered at around 3400 cm^{-1} assigned to the O−H stretching of the H_2O molecules, confirming their hydrated character. In addition, some of the complexes show narrow and broad absorption bands at 3600 and 3300 cm^{-1}, suggesting the presence of either coordination or hydration H_2O molecules, respectively.[47] Moreover, the absorption peaks observed in the

range of 600 to 1000 cm^{-1} are assigned to the vibration of C−C bonds. Except for the OXA complexes, all the complexes present peaks around 2800–3000 cm^{-1} attributed to the C−H vibration and their relative absorption intensity increases with the number of carbon atoms in the chain.

The coordination modes of the carboxylate groups for a given metal ion can be inferred by the difference between the COO^- asymmetric and symmetric modes ($\Delta v = v_{as.} - v_{sym.}$)[48] when compared with the respective Na_2L salt. For $[Eu_2(L)_3(H_2O)_x]\cdot y(H_2O)$ complexes, two distinct absorption peaks were assigned to the $v_{as.}(COO^-)$, suggesting two different coordination modes. The Δv value at around 97 cm^{-1} is associated with a bridge coordination mode, while the Δv value at 130 cm^{-1} is assigned to the chelate coordination mode. The results indicate that the carboxylate groups are coordinated to the Eu^{3+} ions by a mixed bridge-chelate coordination mode, except for the complex with OXA ligand.

The XRD (Powder) patterns of $[Ln_2(L)_3(H_2O)_x]\cdot y(H_2O)$ complexes (L: $^-OOC(CH_2)_{n-2}COO^-$, 2 ≤ n ≤ 12) present highly intense and narrow diffraction peaks predominantly at lower angles (Figure S4), suggesting highly crystalline compounds and large crystallite sizes. The diffractogram profiles of Eu^{3+} and Gd^{3+} complexes are similar, suggesting an isomorphic form when containing the same ligand as reported in literature.[32,49–52]

The similarity of $[Ln_2(OXA)_3(H_2O)_6]\cdot 4(H_2O)$ diffractograms and the standard crystal structure data (CCDC: 816524) confirms a nine-coordinated site with a tricapped trigonal prism geometry[32] (Figure S4). The diffractograms of the complexes with L = MAL, ADP, SUB, and SEB are comparable to their respective standard crystal structure data, CCDC: 181893,[50] 721892,[49] 700675,[51] and 745638,[52] respectively. These results indicate a mixed bridge-chelate Ln^{3+}−L coordination mode as discussed in the FTIR data, even for the MAL ligand that forms chelate rings with 4 and 6 members. It is noteworthy that the XRD patterns obtained from the PIM, AZL, UND, and DOD complexes are reported in this work.

LMCT and Triplet State of Ln^{3+} Complexes

The use of the La^{3+} ion is useful to establish LMCT when compared with those analogues Eu^{3+}–complexes. La^{3+}–complexes are used for obtaining the ligand-to-metal charge transfer state (LMCT) due to the fact that no 4f-4f transitions can be observed. In this sense, the La^{3+}–complexes reflectance spectra can be compared to those analogues of Eu^{3+}–complexes.[53] Moreover, the La^{3+} ion presents an ionic radius (1.216 Å) similar to the ionic radius of the Eu^{3+} ion (1.120 Å).[54]

Diffuse reflectance spectra of the $[Ln_2(L)_3(H_2O)_x]\cdot y(H_2O)$ complexes (Ln: La^{3+} and Eu^{3+}) were recorded in the UV–Vis range (220–600 nm), using $BaSO_4$ as a reflecting standard (Figure S5). When the absorption spectra of the La^{3+} and Eu^{3+} complexes are compared in the range of 220–300 nm, only the broad absorption bands for the Eu^{3+} complexes assigned to LMCT transitions can be observed.[53,55] Also, the absorption spectral profiles of different Eu^{3+} complexes are quite similar, although the energy of the LMCT bands varies as a function of the chemical environment around the metal ion. Besides this, the diffuse reflectance spectra of $[Eu_2(L)_3(H_2O)_x]y(H_2O)$ complexes exhibit narrow absorption peaks assigned to the intraconfigurational transitions of the Eu^{3+} ion (in cm^{-1}): $^7F_0\rightarrow{}^5H_3$ (31446), $^7F_0\rightarrow{}^5D_4$ (27624), $^7F_0\rightarrow{}^5G_5$ (26316), $^7F_0\rightarrow{}^5L_6$ (25316), $^7F_1\rightarrow{}^5D_3$ (24038), $^7F_0\rightarrow{}^5D_2$ (21522), $^7F_{0,1}\rightarrow{}^5D_1$ (19028, 18674), and $^7F_1\rightarrow{}^5D_0$ (16909)

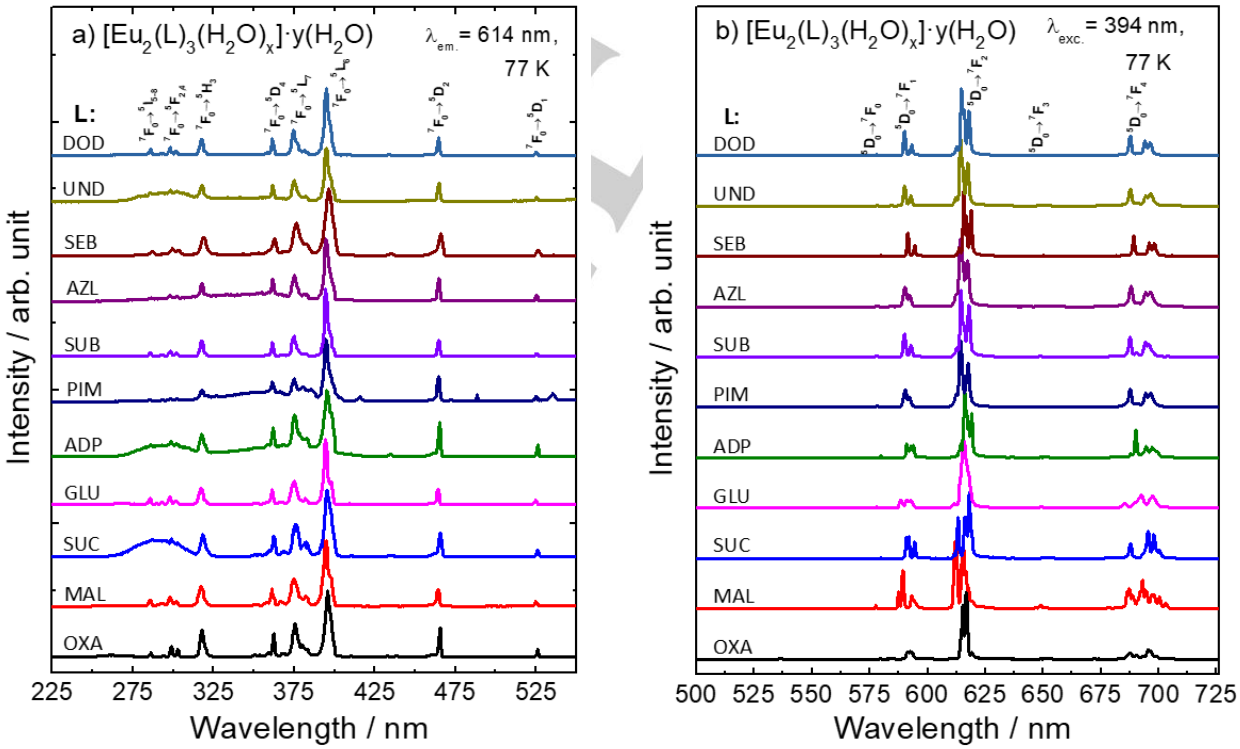

Figure 4. Excitation (a) and emission (b) spectra of the $[Eu_2(L)_3(H_2O)_x]\cdot y(H_2O)$ complexes with aliphatic dicarboxylate ligands (L: $^-OOC(CH_2)_{n-2}COO^-$, 2 ≤ n ≤ 12, x = 2–6 and y = 0–4) measured at 77 K. The excitation spectra were recorded monitoring at the $^5D_0 \rightarrow {}^7F_2$ transition (~ 614 nm). The emission spectra were recorded under excitation at the $^7F_0\rightarrow{}^5L_6$ transition (~394 nm).

The Gd^{3+} ion presents a very large energy gap (32000 cm^{-1}) between the $^8S_{7/2}$ ground state and the first $^6P_{7/2}$ excited state and can be used to estimate the triplet state energies (T_1) of the carboxylate ligands. Thus, Gd^{3+} complexes are useful to understand the energy level structure of the coordinated ligands, especially on the triplet (T_1) energy levels. The Gd^{3+} ion can act simulating the chemical environment of the Eu^{3+} owing to the similarity of their ionic radii ($r_{Gd^{3+}}$ = 1.107 Å).[36,54]

The phosphoresce spectra of $[Gd_2(L)_3(H_2O)_x]\cdot y(H_2O)$ complexes exhibit broad emission bands with barycenters at around 22900 cm^{-1} assigned to the $T_1 \rightarrow S_0$ transitions from carboxylate ligands (Figure S6). The higher energy values of the T_1 states could be assigned to the absence of π conjugated bonds.[56]

Luminescence Properties of the Eu^{3+} Complexes

The excitation (Figure 4a) and emission (Figure 4b) spectra of the $[Eu_2(L)_3(H_2O)_x]\cdot y(H_2O)$ complexes were recorded at 77 K.

The excitation spectra of the $[Eu_2(L)_3(H_2O)_x]\cdot y(H_2O)$ complexes (Figure 4a) recorded in the range of 225–550 nm monitoring the emission of the $^5D_0 \rightarrow {}^7F_2$ transition (~614 nm) show broad absorption bands at ~280 nm assigned to the $S_0 \rightarrow S_1$ intraligand and LMCT states. Moreover, there are narrow absorption bands arising from intraconfigurational transitions of the Eu^{3+} ion (cm^{-1}): $^7F_0 \rightarrow {}^5I_4$ (35088), $^5I_6$ (34130), $^5F_2$ (33557), $^5F_4$ (33112), $^5H_7$ (30675), $^5L_{10}$ (28571), $^5D_4$ (27778), $^5L_7$ (26667), $^5G_4$ (25907), $^5L_6$ (25316), $^5D_3$ (24331), $^5D_2$ (21552), $^5D_1$ (19048), and $^5D_0$ (17241).[25] The excitation spectra recorded at 300 K also exhibit absorption bands arising from the $^7F_1$ and $^7F_2$ excited energy levels (Figure S7) due to energy gap between these energy levels and the $^7F_0$ ground level, that are close to 380 and 1040 cm^{-1}, respectively.[25] These spectral results suggest a thermal dependent population of the excited levels. In general, the 4f-4f transitions arising from the $^7F_1$ and $^7F_2$ levels are not observed for spectra recorded at a low temperature.

The emission spectra of $[Eu_2(L)_3(H_2O)_x]\cdot y(H_2O)$ complexes recorded from 500 to 725 nm (Figure 4b), under excitation at the transition $^7F_0 \rightarrow {}^5L_6$ (~394 nm) show narrow emission bands assigned to the $^5D_0 \rightarrow {}^7F_J$ transitions of the Eu^{3+} ion (in cm^{-1}): $^5D_0 \rightarrow {}^7F_0$ (17227), $^5D_0 \rightarrow {}^7F_1$ (16848), $^5D_0 \rightarrow {}^7F_2$ (16184), $^5D_0 \rightarrow {}^7F_3$ (15331), and $^5D_0 \rightarrow {}^7F_4$ (14358). These emission spectra present only one emission peak attributed to the $^5D_0 \rightarrow {}^7F_0$ (~578 nm), suggesting a unique symmetry site around the Eu^{3+} ion (C_{nv}, C_n or C_s).[36] It is important to emphasize that the excitation is monitored on the $^5L_6$ of the Eu^{3+} ion, which is far from the ligand singlet state.

Experimental Intensity Parameters

The odd–even effect due to the dicarboxylate chemical environment around the Eu^{3+} ion was observed in the experimental intensity parameters Ω_2 and Ω_4, as shown in Figure 5. Since it is not possible to distinguish the contributions of the forced electric dipole and dynamic coupling mechanisms in the experimental Ω_2 and Ω_4 intensity parameters, it is extremely important to have a theoretical detailed description of these parameters,[57] as it will be discussed in the following section.

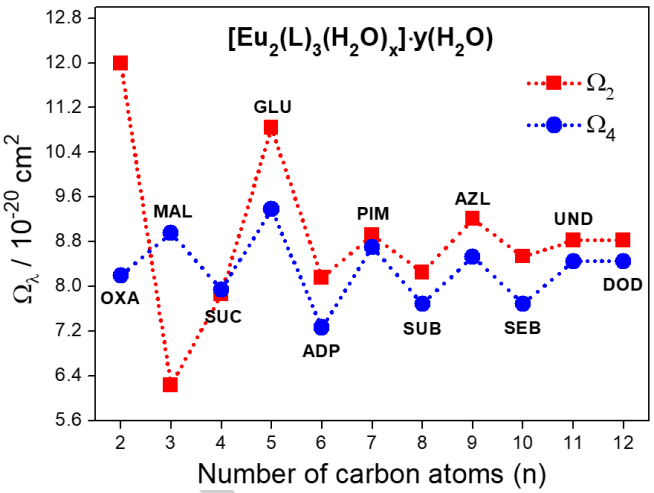

Figure 5. Odd–even effect on the experimental intensity parameters Ω_2 (red squares) and Ω_4 (blue circles) of the $[Eu_2(L)_3(H_2O)_x]\cdot y(H_2O)$ complexes as a function of the number of carbon atoms (n) in the dicarboxylate ligand chain (L: $^-OOC(CH_2)_{n-2}COO^-$, $2 \le n \le 12$, x = 2–6 and y = 0–4).

Theoretical Intensity Parameters

For calculation of the theoretical intensity parameters (Ω_λ), the experimental crystallographic data of the coordination compounds were used to generate reduced unit cells that simulate the total system, according to Figure 6. The crystallographic unit cell was replicated in a size enough to extract the total structure of the $[Eu_2(L)_3(H_2O)_x]\cdot y(H_2O)$ complexes (Figures 6a and 6b). These structures, as a function of the number of carbon atoms (n) in the dicarboxylate ligand chain (L: $^-OOC(CH_2)_{n-2}COO^-$, $2 \le n \le 12$), were isolated to build up proper unit cells (Figure 6b), that were used to perform all geometry optimizations using Periodic Boundary Conditions (PBC). From the optimized structures, the ligand geometries were taken out (isolated) to calculate the ligand effective polarizabilities (α').

The theoretical PBC equilibrium geometries were calculated for all the Eu^{3+} complexes and compared with the experimental crystallographic data, as available in literature. All calculated geometries are quite similar to the crystallographic ones with root-mean-square deviation ~0.475 Å (Table S2 and Figure S8). The coordination polyhedron is formed by a Eu^{3+} ion bridged to a second Eu^{3+} ion by two ligands, each one with a μ_2-oxygen carboxylate shared by the dimer (Figure 6d), with exception of the Eu^{3+}–OXA complex.

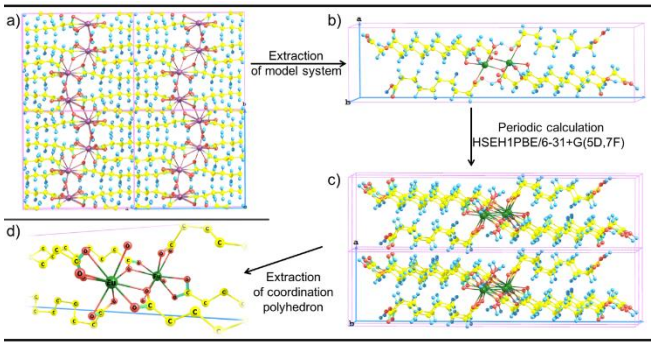

Figure 6. Schematic replication of crystallographic unit cell (a) used to build up the reduced unit cell (b) for the PBC calculations (c). The coordination polyhedron (d) was extracted to carry out the theoretical Ω_λ intensity parameters calculations.

The coordination mode of the ligands plays an important role in the determination of effective polarizability calculations (α'). The ligand structures and the superposition of LMOs of the coordination carboxylate group are depicted in Figure 7.

The dicarboxylate ligand with n = 2 (OXA) acts as a bidentate chelating ligand with an oxygen atom from each carboxylate group. The malonate ligand n = 3 (MAL) also acts as a bidentate chelating ligand. However, coordination can occur either with one oxygen atom from each carboxylate group or with the two oxygen atoms from one of the carboxylate groups (Figure 7b). For the organic ligands with n ≥ 4, the coordination occurs with the two oxygen atoms from the same carboxylate group (Figure 7c).

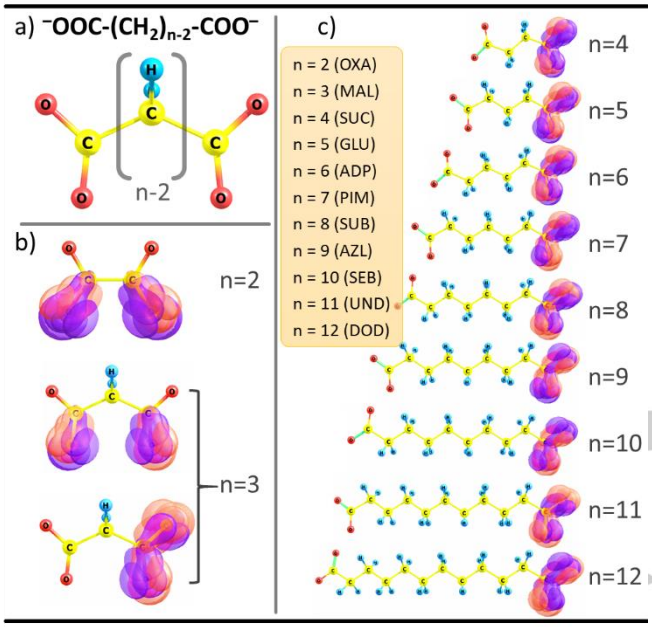

Figure 7. Ligand structures and the superposition of LMOs in the coordination carboxylate groups in different types of coordination.

The molecular isotropic polarizability (α_{mol}) for all the ligand structures was calculated, as well as their decompositions in the LMOs contributions (Table 1). Using the decomposed α_{mol} it is possible to extract the coordinated carboxylate polarizability ($\alpha_{CO_2^-}$), which contributes with two ligating atoms. Therefore, the ligand effective polarizability (one ligating atom contribution) is taken as $\alpha' = \alpha_{CO_2^-}/2$. The Ghost-Atom polarizability α^* is obtained from Eq. (11).

The odd–even effect can be observed in Figure 8, where the permanent dipoles (red squares) and the GA polarizabilities (blue triangles) have opposite trends. In the cases where the values of $|\vec{\mu}_P| \neq 0$ (n = odd), the ligands have a net charge separation. Therefore, the odd carbon members have a more rigid electron density and smaller values of α^* than in the cases of the even carbon members.

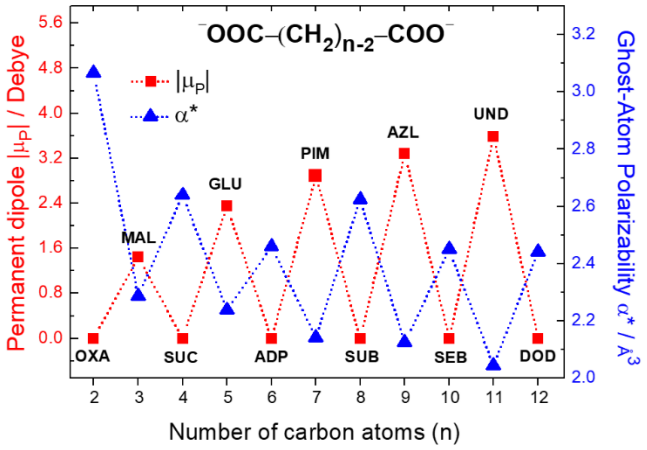

Figure 8. Calculated permanent dipole moment $\vec{\mu}_P$ (red squares) and the ghost-atom polarizability α^* (blue triangles) for each ligand. These values are in function of the number of carbons in the chain (2 ≤ n ≤ 12).

Table 1. Molecular isotropic polarizabilities (α_{mol}), the carboxylate isotropic polarizabilities ($\alpha_{CO_2^-}$), ligand effective polarizabilities (α'), and Ghost–Atom polarizabilities (α^*). The polarizabilities are in Å^3.

n	α_{mol}	$\alpha_{CO_2^-}$	α' [(a)]	α^*
2	9.443	2.506	1.253	3.067
3	11.852	2.272	1.136	2.286
4	13.354	2.258	1.129	2.640
5	15.272	2.142	1.071	2.237
6	17.045	2.164	1.082	2.460
7	18.973	2.176	1.088	2.141
8	20.869	2.200	1.100	2.625
9	22.812	2.206	1.103	2.124
10	24.741	2.234	1.117	2.450
11	26.694	2.234	1.117	2.044
12	28.637	2.216	1.108	2.441

[(a)] $\alpha' = \overline{\alpha}_{CO_2^-}/2$

As can be seen in Figure S9 and Table 1, α' values do not follow an odd–even effect, whereas α^* values have variations between odd and even ligands. These variations in the polarization of the ligands, represented by the Ghost–Atom (as illustrated in Figure 9), reflects in the changes of the $^5D_0 \rightarrow {}^7F_J$ transitions by the DC mechanism.

Table S5 and Figure 10 show that the Ω_λ theoretical intensities parameter values are in a good agreement with the experimental ones. The FED mechanism participation at around 4% for Ω_2 and 12% for Ω_4 is less representative than the DC mechanism, where calculated α' and estimated α^* are used (Approach A). The inclusion of the Ghost–Atom in the calculations decreases the average relative errors with respect to the experimental values, from 18% (Approach B) to 7% (Approach A).

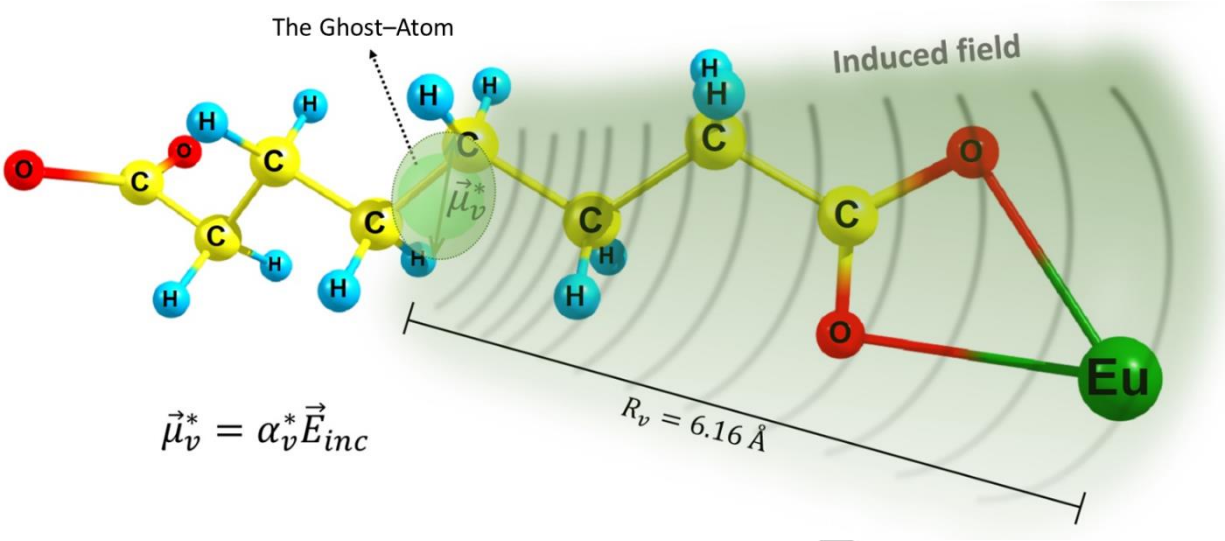

Figure 9. Representation of the long-range interaction accounted for by the Ghost-Atoms included in each ligand, emphasizing the dipole effectively induced by the ligand long chains.

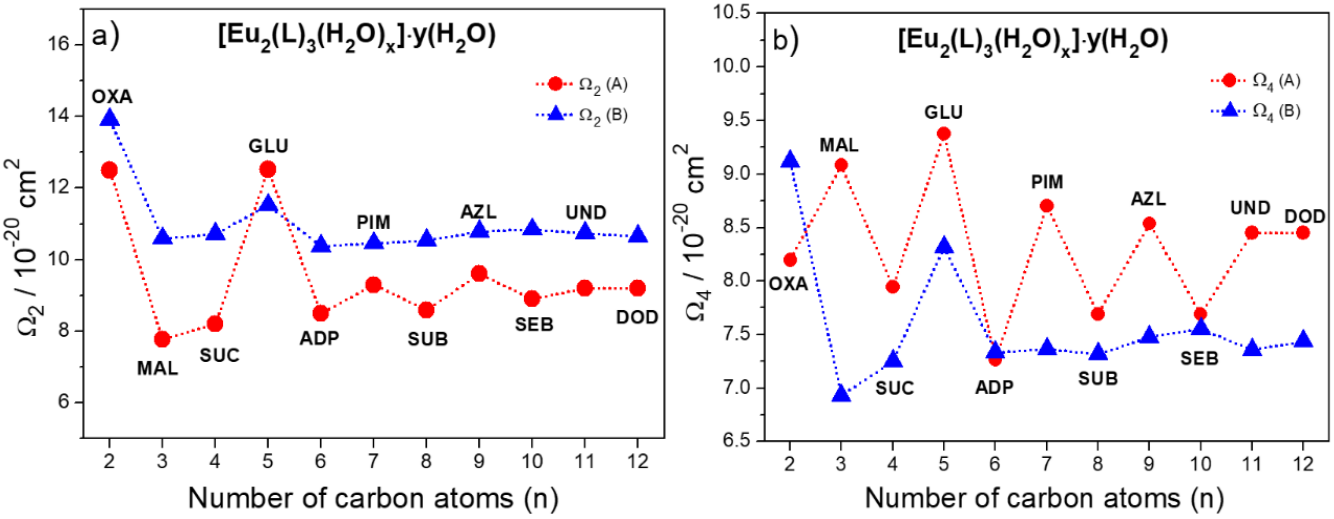

Figure 10. Odd–even effect on the theoretical intensity parameters Ω_2 (a) and Ω_4 (b) of the $[Eu_2(L)_3(H_2O)_x]\cdot y(H_2O)$ complexes as a function of the number of carbon atoms (n) in the dicarboxylate ligands (L: $^-OOC(CH_2)_{n-2}COO^-$, $2 \le n \le 12$). In both cases, the theoretical Ω_λ (A) were obtained with the inclusion of the Ghost–Atom polarizability, while the Ω_λ (B) were obtained without this effect.

Intrinsic Quantum Yield

The lifetime (τ) values of the $^5D_0$ emitting level of the $[Eu_2(L)_3(H_2O)_x]\cdot y(H_2O)$ complexes were obtained from the luminescence decay curves registered at room temperature (Figure S10), monitoring the emission of the $^5D_0 \rightarrow {}^7F_2$ transition (~615 nm) with an excitation wavelength at the $^7F_0 \rightarrow {}^5L_6$ transition (~394 nm). The lifetime values for all complexes range from 0.36 to 0.64 ms, except for the $[Eu_2(OXA)_3(H_2O)_6]\cdot 4(H_2O)$ and $[Eu_2(MAL)_3(H_2O)_6]$ complexes that present the lowest τ values, 0.31 and 0.30 ms, respectively (Table S5). These lower values are attributed to the presence of the highest number of water molecules in the first coordination sphere (three water molecules per Eu^{3+} ion). The $[Eu_2(SUC)_3(H_2O)_2]\cdot H_2O$ complex presents the highest value of lifetime (0.639 ms), due to the lowest water molecule number and multiphonon relaxation by coupling with the O–H oscillators.

Furthermore, the lifetime data are useful for determining the number of water molecules in the first coordination sphere around the Eu^{3+} ion, *i*.e. the hydration degree or hydration number (q_{H_2O}).[25] In order to obtain these values, Eq. (13) was used, which leads to values with estimated errors of about ± 0.5 water molecule per Eu^{3+} ion.[25,58,59]

$$q_{H_2O} = 1.05\frac{1}{\tau} - 0.70 \qquad (13)$$

The number of coordinated H_2O molecules to the Eu^{3+} ion calculated by Eq. (13) usually present fractional values, lower than those obtained experimentally. This fact can be due to

different factors, such as the presence of further oscillators different from the O–H mode, the C–H oscillators and the influence of the second coordination sphere that also can lead to a lowering of the lifetime values of the $^5D_0$ emitting level. In this way, the number of coordinated H_2O molecules (Table S5) agrees with the experimental ones obtained by the elemental and thermogravimetric analyses.

The emission intrinsic quantum yield Q_{Ln}^{Ln} (using Bünzli's notation[22]) of the $^5D_0$ emitting level of the Eu^{3+} ion is the ratio between the radiative $\left(A_{rad} = \sum A_{0\to J}\right)$ and the non-radiative (A_{nrad}) + radiative decay processes. Based on the experimental lifetimes of the $^5D_0$ emitting level in Eq. (14), and A_{rad}, calculated from Eq. (3), it is possible to determine the non-radiative A_{nrad} rates and the emission intrinsic quantum yield as given by Eq. (15).

$$A_{tot} = \frac{1}{\tau} = A_{rad} + A_{nrad} \quad (14)$$

$$Q_{Ln}^{Ln} = \frac{A_{rad}}{A_{rad} + A_{nrad}} \quad (15)$$

It is noteworthy that for all the Eu^{3+} complexes containing a ligand with a number of carbon atoms n ≥ 5, the Q_{Ln}^{Ln} values (Figure 11) present the *zigzag* behavior with respect to their number of carbons in the chain. The presence of odd-even effect come from the radiative rate contribution (A_{rad}), while the non-radiative rate (A_{nrad}) is insensitive to the *zigzag* behavior (Figure S11).

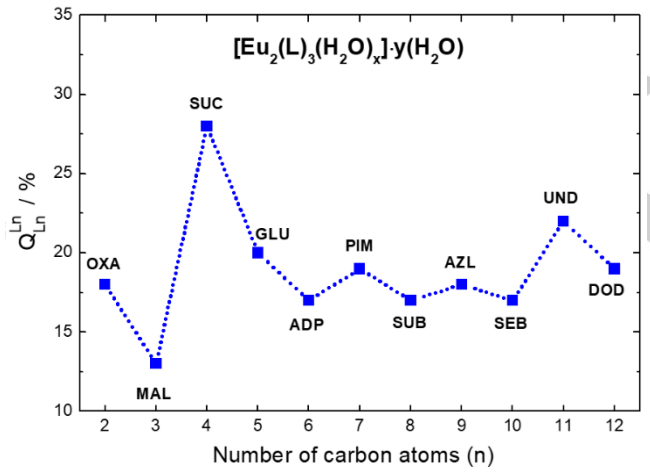

Figure 11. The relationship between the emission intrinsic quantum yield (Q_{Ln}^{Ln}) of the $[Eu_2(L)_3(H_2O)_x]\cdot y(H_2O)$ complexes as a function of the number of carbon atoms (n) in the aliphatic dicarboxylate ligands (L: $^-OOC(CH_2)_{n-2}COO^-$, 2 ≤ n ≤ 12, x = 2–6 and y = 0–4).

Moreover, the total decay rate (A_{tot}), the denominator in Eq. (15) is by far dominated by the non-radiative components. The $[Eu_2(SUC)_3(H_2O)_2]H_2O$ complex presents the highest value of Q_{Ln}^{Ln} (28%), which is in a good agreement with the lowest number of coordinated water molecules compared to the other members of the series (Table S5).

Conclusions

In this work, an odd–even effect systematic study based on photoluminescent properties of eleven Eu^{3+} aliphatic dicarboxylate complexes $[Eu_2(L)_3(H_2O)_x]\cdot y(H_2O)$ (L: OXA, MAL, SUC, GLU, ADP, PIM, SUB, AZL, SEB, UND, and DOD, where x = 2–6 and y = 0–4) was experimentally and theoretically discussed. TG-DTG data indicate a *zigzag* pattern in the dehydration process in which the H_2O molecules are released at lower temperatures for the odd carbon members of the series than the even ones, showing the odd–even effect.

Besides, a "Ghost-Atom" model was introduced to simulate the long-range dispersion effects of the ligand chain on the first coordination sphere of the Eu^{3+} dicarboxylate complexes. The Ω_2 and Ω_4 theoretical and experimental intensity parameters values and *zigzag* patterns (odd–even effect) were in almost complete agreement, the theoretical values being efficiently described by the Ghost–Atom model. The intrinsic quantum yield (Q_{Ln}^{Ln}) of the Eu^{3+} complexes also presents the odd–even effect due to the radiative rate A_{rad} that depend straightly on the Ω_λ intensity parameters, indicating that the Eu^{3+} ion acts as a powerful luminescent probe for chemical environment around lanthanide ion.

Finally, the *zigzag* patterns from the photoluminescence features of Eu^{3+} dicarboxylate complexes were experimentally observed and successfully explained based on theoretical approaches of the 4f-4f transition intensities, confirming the odd–even effect.

Acknowledgements

The authors thank the funding agencies for financial support: Conselho Nacional de Desenvolvimento Científico e Tecnológico (CNPq), Fundação de Amparo à Pesquisa do Estado de São Paulo (FAPESP).

Keywords: The odd–even effect • europium • dicarboxylate complexes • photoluminescence intensity parameters

References

[1] R. Janicki, A. Mondry, P. Starynowicz, *Coord. Chem. Rev.* **2017**, *340*, 98–133.

[2] C. N. R. Rao, S. Natarajan, R. Vaidhyanathan, *Angew. Chem. Int. Ed.* **2004**, *43*, 1466–1496.

[3] V. R. Thalladi, M. Nüsse, R. Boese, *J. Am. Chem. Soc.* **2000**, *122*, 9227–9236.

[4] F. Tao, S. L. Bernasek, *Chem. Rev.* **2007**, *107*, 1408–1453.

[5] M. K. Mishra, S. Varughese, U. Ramamurty, G. R. Desiraju, *J. Am. Chem. Soc.* **2013**, *135*, 8121–8124.

[6] K. Yang, Z. Cai, A. Jaiswal, M. Tyagi, J. S. Moore, Y. Zhang, *Angew. Chem. Int. Ed.* **2016**, *55*, 14090–14095.

[7] L. P. De La Rama, L. Hu, Z. Ye, M. Y. Efremov, L. H. Allen, *J. Am. Chem. Soc.* **2013**, *135*, 14286–14298.

[8] E. R. Dionne, C. Dip, V. Toader, A. Badia, *J. Am. Chem. Soc.* **2018**, *140*, 10063–10066.

[9] N. Varghese, G. S. Shetye, S. Yang, S. Wilkens, R. P. Smith, Y. Y. Luk, *J. Colloid Interface Sci.* **2013**, *412*, 95–99.

[10] R. Marty, R. Nigon, D. Leite, H. Frauenrath, *J. Am. Chem. Soc.* **2014**, *136*, 3919–3927.
[11] Y. Feng, E. R. Dionne, V. Toader, G. Beaudoin, A. Badia, *J. Phys. Chem. C* **2017**, *121*, 24626–24640.
[12] M. Dendzik, A. Terfort, P. Cyganik, *J. Phys. Chem. C* **2012**, *116*, 19535–19542.
[13] L. Jiang, C. S. S. Sangeeth, C. A. Nijhuis, *J. Am. Chem. Soc.* **2015**, *137*, 10659–10667.
[14] M. Baghbanzadeh, F. C. Simeone, C. M. Bowers, K. C. Liao, M. Thuo, M. Baghbanzadeh, M. S. Miller, T. B. Carmichael, G. M. Whitesides, *J. Am. Chem. Soc.* **2014**, *136*, 16919–16925.
[15] H. Aitchison, H. Lu, S. W. L. Hogan, H. Früchtl, I. Cebula, M. Zharnikov, M. Buck, *Langmuir* **2016**, *32*, 9397–9409.
[16] K. Binnemans, *Chem. Rev.* **2009**, *109*, 4283–4374.
[17] J. Rocha, L. D. Carlos, F. A. A. Paz, D. Ananias, *Chem. Soc. Rev.* **2011**, *40*, 926–940.
[18] J. C. G. Bünzli, *Coord. Chem. Rev.* **2015**, *293–294*, 19–47.
[19] U. Mueller, M. Schubert, F. Teich, H. Puetter, K. Schierle-Arndt, J. Pastré, *J. Mater. Chem.* **2006**, *16*, 626–636.
[20] U. Ravon, M. E. Domine, C. Gaudillère, A. Desmartin-Chomel, D. Farrusseng, *New J. Chem.* **2008**, *32*, 937.
[21] C. N. Banti, S. K. Hadjikakou, *Eur. J. Inorg. Chem.* **2016**, *2016*, 3048–3071.
[22] S. V. Eliseeva, J. C. G. Bünzli, *Chem. Soc. Rev.* **2010**, *39*, 189–227.
[23] S. Cotton, *Lanthanide and Actinide Chemistry*, John Wiley & Sons, Ltd, Chichester, UK, **2006**.
[24] G. F. de Sá, O. L. Malta, C. de Mello Donegá, A. M. Simas, R. L. Longo, P. A. Santa-Cruz, E. F. da Silva, *Coord. Chem. Rev.* **2000**, *196*, 165–195.
[25] K. Binnemans, *Coord. Chem. Rev.* **2015**, *295*, 1–45.
[26] D. Mustafa, I. G. N. Silva, S. R. Bajpe, J. A. Martens, C. E. A. Kirschhock, E. Breynaert, H. F. Brito, *Dalt. Trans.* **2014**, *43*, 13480–13484.
[27] Z. Amghouz, S. García-Granda, J. R. García, R. a S. Ferreira, L. Mafra, L. D. Carlos, J. Rocha, *Inorg. Chem.* **2012**, *51*, 1703–1716.
[28] N. Stock, S. Biswas, *Chem. Rev.* **2012**, *112*, 933–969.
[29] O. L. Malta, *Chem. Phys. Lett.* **1982**, *88*, 353–356.
[30] O. L. Malta, *Chem. Phys. Lett.* **1982**, *87*, 27–29.
[31] R. T. Moura Jr, A. N. Carneiro Neto, R. L. Longo, O. L. Malta, *J. Lumin.* **2016**, *170*, 420–430.
[32] T.-F. Liu, W. Zhang, W.-H. Sun, R. Cao, *Inorg. Chem.* **2011**, *50*, 5242–8.
[33] F.-Y. Yi, W. Zhu, S. Dang, J.-P. Li, D. Wu, Y. Li, Z.-M. Sun, *Chem. Commun.* **2015**, *51*, 3336–3339.
[34] K. Nagase, H. Yokobayashi, K. Muraishi, M. Kikuchi, *Thermochim. Acta* **1991**, *177*, 273–284.
[35] O. L. Malta, M. A. Couto Dos Santos, L. C. Thompson, N. K. Ito, *J. Lumin.* **1996**, *69*, 77–84.
[36] H. F. Brito, O. M. L. Malta, M. C. F. C. Felinto, E. E. S. Teotonio, in *PATAI'S Chem. Funct. Groups*, John Wiley & Sons, Ltd, Chichester, UK, **2010**.
[37] W. T. Carnall, H. Crosswhite, H. M. Crosswhite, *Energy Level Structure and Transition Probabilities in the Spectra of the Trivalent Lanthanides in LaF_3*, Argonne, IL (United States), IL (United States), **1978**.
[38] B. R. Judd, *Phys. Rev.* **1962**, *127*, 750–761.
[39] G. S. Ofelt, *J. Chem. Phys.* **1962**, *37*, 511–520.
[40] C. K. Jørgensen, B. R. Judd, *Mol. Phys.* **1964**, *8*, 281–290.
[41] S. F. Mason, R. D. Peacock, B. Stewart, *Mol. Phys.* **1975**, *30*, 1829–1841.
[42] B. R. Judd, *J. Chem. Phys.* **1979**, *70*, 4830.
[43] A. N. Carneiro Neto, R. T. Moura, E. C. Aguiar, C. V. Santos, M. A. F. L. B. de Medeiros, *J. Lumin.* **2018**, *201*, 451–459.
[44] O. L. Malta, H. J. Batista, L. D. Carlos, *Chem. Phys.* **2002**, *282*, 21–30.
[45] J. J. Dallara, M. F. Reid, F. S. Richardson, *J. Phys. Chem.* **1984**, *5735*, 3587–3594.
[46] J. Pipek, P. G. Mezey, *J. Chem. Phys.* **1989**, *90*, 4916–4926.
[47] C. A. F. De Oliveira, F. F. Da Silva, I. Malvestiti, V. R. D. S. Malta, J. D. L. Dutra, N. B. Da Costa, R. O. Freire, S. Alves, *J. Mol. Struct.* **2013**, *1041*, 61–67.
[48] G. B. Deacon, R. J. Phillips, *Coord. Chem. Rev.* **1980**, *33*, 227–250.
[49] Y.-B. Ding, X.-H. Shi, Y. Cheng, J. Zhang, Y.-G. Yin, W.-H. Gao, *Inorg. Chem. Commun.* **2009**, *12*, 695–697.
[50] M. Hernández-Molina, P. Lorenzo-Luis, C. Ruiz-Pérez, T. López, I. R. Martín, K. M. Anderson, A. G. Orpen, E. H. Bocanegra, F. Lloret, M. Julve, *J. Chem. Soc. Dalt. Trans.* **2002**, *2*, 3462–3470.
[51] D. T. d. Lill, A. M. Tareila, C. L. Cahill, *Inorg. Chem. Commun.* **2009**, *12*, 191–194.
[52] Y. Xie, F. Y. Bai, Y. H. Xing, Z. Wang, Z. F. Pu, M. F. Ge, *J. Inorg. Organomet. Polym. Mater.* **2010**, *20*, 258–263.
[53] L. D. Carlos, J. A. Fernandes, R. A. S. Ferreira, O. L. Malta, I. S. Gonçalves, P. Ribeiro-Claro, *Chem. Phys. Lett.* **2005**, *413*, 22–24.
[54] R. D. Shannon, *Acta Crystallogr. Sect. A* **1976**, *32*, 751–767.
[55] W. M. Faustino, O. L. Malta, G. F. de Sá, *J. Chem. Phys.* **2005**, *122*, 054109.
[56] N. Filipescu, W. Sager, F. Serafin, *J. Phys. Chem.* **1964**, *68*, 3324–3346.
[57] O. L. Malta, H. F. Brito, J. F. S. Menezes, F. R. G. e Silva, S. Alves, F. S. Farias, A. V. M. de Andrade, *J. Lumin.* **1997**, *75*, 255–268.
[58] P. P. Barthelemy, G. R. Choppin, *Inorg. Chem.* **1989**, *28*, 3354–3357.
[59] R. M. Supkowski, W. D. Horrocks, *Inorganica Chim. Acta* **2002**, *340*, 44–48.

WILEY-VCH

FULL PAPER

Entry for the Table of Contents

FULL PAPER

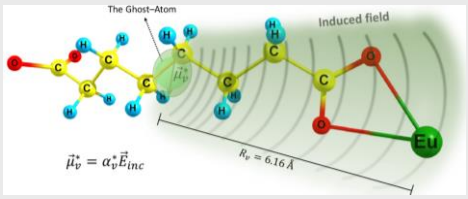

Israel P. Assunção, Albano N. Carneiro Neto, Renaldo T. Moura Jr., Cássio C. S. Pedroso, Ivan G. N. Silva, Maria C.F.C. Felinto, Ercules E.S. Teotonio, Oscar L. Malta and Hermi F. Brito**

Pages 1 – 10.

Odd–Even Effect on Luminescence Properties of Europium Aliphatic Dicarboxylate Complexes